

# Cooper-Paired Bipolaronic Superconductors

M. Grundner <sup>1,2</sup> T. Blatz <sup>1,2</sup> J. Sous <sup>3,4</sup> U. Schollwöck <sup>1,2</sup> and S. Paeckel <sup>1,2</sup>

<sup>1</sup>*Department of Physics and Arnold Sommerfeld Center for Theoretical Physics (ASC), Ludwig-Maximilians-Universität München, D-80333 Munich, Germany*

<sup>2</sup>*Munich Center for Quantum Science and Technology (MCQST), D-80799 München, Germany*

<sup>3</sup>*Department of Physics, Stanford University, Stanford, CA 93405, USA*

<sup>4</sup>*Department of Chemistry and Biochemistry, University of California, San Diego, La Jolla, California 92093, USA*

(Dated: August 28, 2023)

Light-mass bipolarons in off-diagonally coupled electron-phonon systems provide a potential route to bipolaronic high- $T_c$  superconductivity. While there has been numerical progress in the physically relevant limit of slow phonons, more insights are needed to fully understand to what extent this mechanism survives at finite densities and in different regimes. We address these questions using advanced tensor-network methods applied to the Su-Schrieffer-Heeger model. Studying both the spectral properties of isolated bipolarons as well as the pairing correlations at small finite densities, we find evidence that the conventional picture of bipolarons as molecular bound states which undergo Bose-Einstein condensation may need to be reconsidered. Instead, our findings suggest correlation-driven formation of a fragmented condensate with spatially separated polaron pairs, stabilized by strong repulsive electron-electron interactions at moderate values of the electron-phonon coupling. These spatially modulated charge clouds exhibit pairing with a typical length-scale set by the Fermi momentum.

*Introduction* Phonon-mediated high- $T_c$  superconductivity at ambient pressure is a fascinating long-standing theoretical idea challenged by the fact that local (Holstein or Fröhlich) coupling to phonons results in an exponential increase in the quasiparticle mass, suppressing  $T_c$  [1–8]. Nevertheless, recent studies on systems with off-diagonal electron-phonon interaction reported the formation of light-mass, small-size bipolarons [9–15] and estimated large values of  $T_c$ . This analysis is based on the assumption that a gas of bipolarons would undergo a transition to a Bose-Einstein condensate (BEC) at finite densities and that this is not preempted by a competing phase. Numerical simulations of these models are challenging even at  $T = 0$ , for the physically relevant regime of small phonon frequencies  $\Omega$  with adiabaticity ratios  $A = \Omega/2t \ll 1$ , where  $t$  denotes the electronic hopping amplitude. Here, we use projected purified matrix-product state (MPS)-based techniques [16–21] to examine the validity of the assumptions at the example of the prototypical one-dimensional Su-Schrieffer-Heeger (SSH) model in the adiabatic limit. Our results indicate that in contrast to the anti-adiabatic limit  $A > 1$  [9], in one dimension isolated bipolarons are unstable in the presence of finite electron-electron interactions. As a consequence, at finite densities we find that the picture of Bose-Einstein condensation of weakly-interacting molecular bound states does not hold. In turn, we observe the formation of states with dominant Cooper-pairing. Due to strong correlations, these states do not condense into a macroscopically occupied state [22]. Instead, they form a maximally fragmented condensate, a scenario which has been investigated in striped superconductors, only recently, and which suggests a coupling between charge-density modulations with different wave vectors and the superconducting order parameter field [23, 24]. Our findings indicate that dilute superconductors exhibit non-

trivial, strongly-correlated ground states formed of spatially coherent polaron pairs [5, 6].

*Model and Methods* In the adiabatic limit, the energy cost  $\Omega$  to excite phonons is much smaller than the electronic bandwidth, limiting analytical progress. Consequently, unbiased numerical tools are needed to simulate the spectral properties of polarons and bipolarons. There have been significant advances based on various numerical techniques [25–37]. While most of them have been applied successfully to local Holstein or Fröhlich type electron-phonon interactions, here we study the SSH-Hubbard model in one dimension, given by the Hamiltonian

$$\hat{H} = - \sum_{j,\sigma} \left( \hat{c}_{j,\sigma}^\dagger \hat{c}_{j+1,\sigma} + \text{h.c.} \right) \left( t - \alpha \hat{V}_{j,j+1} \right) + U \sum_j \hat{n}_{j,\uparrow} \hat{n}_{j,\downarrow} + \Omega \sum_j \hat{a}_j^\dagger \hat{a}_j, \quad (1)$$

where  $\hat{c}_{j,\sigma}^{(\dagger)}$  are the spin- $\sigma$  electronic ladder operators and  $\hat{a}_j^{(\dagger)}$  denote the annihilation (creation) operators of optical phonons with frequency  $\Omega$ . The interaction is given by  $\hat{V}_{j,j+1} = \sqrt{2M\Omega} \left( \hat{X}_j - \hat{X}_{j+1} \right) = \hat{a}_j^\dagger + a_j - \hat{a}_{j+1}^\dagger - a_{j+1}$  with the phonon displacements  $\hat{X}_j$ , and we choose the oscillator mass  $M = 1$ . A relevant energy scale is set by the dimensionless, effective electron-phonon coupling  $\lambda = \frac{2\alpha^2}{\Omega t}$ . But care must be taken when tuning  $\lambda$ . Since Eq. (1) is obtained by neglecting higher order couplings, one must restrict the model to the linear approximation in which the displacements do not induce a sign change of the hopping integral [38, 39]; we have confirmed that this is the case in our simulations [40].

We use MPS [16, 17, 41–43] representations tailored to describe large local Hilbert spaces [20, 21]. In order to calculate spectral functions, we combine those with improved time-evolution schemes [18, 19, 40]. We obtain

the isolated (bi-)polaron spectral functions [44, 45] from the time-dependent Greens functions

$$G_P(j, t) = \langle \emptyset | \hat{c}_{j,\sigma}(t) \hat{c}_{L/2,\sigma}^\dagger(0) | \emptyset \rangle \quad \text{polaron}, \quad (2)$$

$$G_{BP}(j, t) = \langle \emptyset | \hat{d}_j^\dagger(t) \hat{d}_{L/2}^\dagger(0) | \emptyset \rangle \quad \text{bipolaron}, \quad (3)$$

where  $|\emptyset\rangle$  denotes the combined electron-phonon vacuum state and  $\hat{d}_j^{(\dagger)} = (\hat{c}_{j,\downarrow} \hat{c}_{j,\uparrow})^{(\dagger)}$  the two-particle electronic operators. Taking two Fourier transformations yields the momentum resolved spectral functions  $S_\alpha(k, \omega)$  with  $\alpha = P, BP$ . We complement the investigations of isolated bipolarons by studying the ground state of the SSH model at small electronic fillings  $n = N/2L \sim 0.1$ . Here, the opening of a spin gap turns the ground state into a Luther-Emery liquid [46, 47] with dominant pairing correlations. An in-depth analysis of the phase diagram at small densities is beyond the scope of this work; here we focus on a careful characterization of the electron pairing. For that purpose, we investigate the two-particle reduced density-matrix (2RDM) in the spin-singlet pairing-channel

$$\hat{\rho}^{(2)} = \sum_{ijmn} \rho_{(ij),(mn)} \hat{c}_{i,\uparrow}^\dagger \hat{c}_{j,\downarrow}^\dagger \hat{c}_{m,\downarrow} \hat{c}_{n,\uparrow}, \quad (4)$$

with the 2RDM matrix elements  $\rho_{(ij),(mn)} = \langle \psi | \hat{c}_{i,\uparrow}^\dagger \hat{c}_{j,\downarrow}^\dagger \hat{c}_{m,\downarrow} \hat{c}_{n,\uparrow} | \psi \rangle$ . Note that for the case of Bose-Einstein condensation, one typically studies only the on-site contributions  $\rho_{(ij),(mn)}^{\text{BEC}} = \rho_{(ij),(mn)} \delta_{ij} \delta_{mn}$ . The full algorithmic details as well as investigations of model instabilities are provided in [40].

*Spectral properties of (bi-)polarons in the SSH model*  
We begin our analysis by studying the quasi-particle dispersion relations of isolated polarons and bipolarons, extracted from the spectral functions  $S_\alpha(k, \omega)$ . We show two-electron spectral functions in Fig. 1, calculated for a system of  $L = 256$  lattice sites. Fitting the position of maxima in line-cuts at constant momentum  $k$  and in the lowest peak of  $S_{P/BP}(k, \omega)$  [40], we determine the quasi-particle dispersion relation  $\varepsilon_{P/BP}(k) = \varepsilon_{P/BP}^0 + \frac{k^2}{2m_{\text{eff}}}$  near  $k = 0$  with the quasi-particle effective mass  $m_{\text{eff}} = \left. \frac{\partial^2 E}{\partial k^2} \right|_{k=0}$  and the ground-state energy  $\varepsilon_{P/BP}^0$ . Introducing the bipolaronic binding energy

$$\Delta_{BP}(k) = \varepsilon_{BP}(k) - 2\varepsilon_P(k), \quad (5)$$

we call two-electron states stable bipolarons if  $\Delta_{BP}(k) < 0$ . Note that for all values of  $\lambda$  investigated, we find the minimum of the polaron dispersion relation to be located at  $k_P = 0$ , i.e., deep in the adiabatic limit we do not observe a transition to a finite-momentum polaron ground state for  $\lambda \leq 1.5$  [48–51]. First, we note in Figs. 1a and 1b a strong feature at  $k = \pi$ , which can be attributed to unstable, localized on-site bipolaron-like states [40]. The extracted bipolaronic binding energies are shown in Fig. 1c varying both the electron-phonon and the Hubbard interaction. Strikingly, we do not observe stable bipolarons

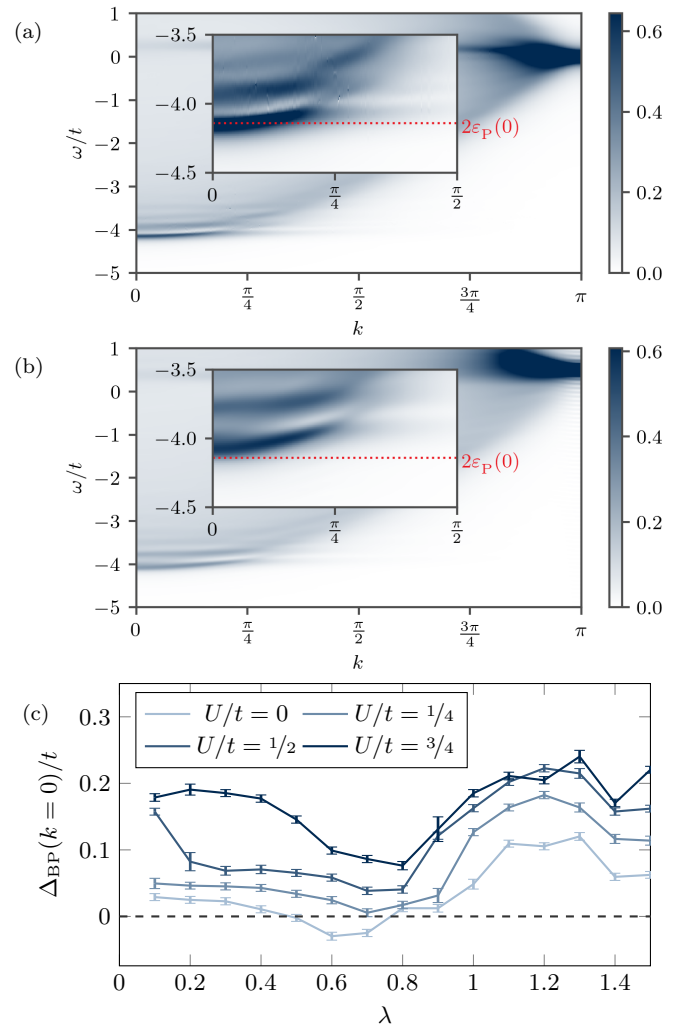


FIG. 1. In (a) we show the pair spectral function for  $U/t = 0, \Omega/t = 0.2$  and  $\lambda = 0.5$ , employing a Lorentzian broadening  $\eta/t = 0.05$ . In the inset we can identify the lowest bipolaronic bound state. We also marked the two-polaron ground-state energy  $2\varepsilon_P(k = 0)$  as dotted line. In (b) we display the case  $U/t = 0.5$ . Here, the bipolaronic spectral function exhibits an incoherent band, i.e., the bipolarons are unstable towards decaying into two-polaron states. In (c), the extracted bipolaronic binding energies  $\Delta_{BP}(k) = 2\varepsilon_{BP}(k) - \varepsilon_P(k)$  as a function of electron-phonon coupling  $\lambda$  are shown. We observe stable bipolarons only for  $U/t = 0$  in a small range of electron-phonon couplings  $\lambda \in [0.5, 0.7]$ .

except for a small region  $\lambda \in [0.5, 0.7]$  for non-interacting electrons  $U/t = 0$ . Figure 1b illustrates this finding for the case of  $U/t = 0.5$ : There is only a broad, incoherent band around  $\omega/t \sim -4.1$  indicating the decay of bipolarons into polarons that form a continuum, marked by the dashed, red line in the inset. Nevertheless, the overall energy differences between polaronic and bipolaronic ground states are very small  $\Delta_{BP}/t \sim 0.1$ , indicating that at finite fillings correlation effects may play a crucial role. Note that in order to connect to previous works we also considered the anti-adiabatic regime  $\Omega/t = 1$ . In

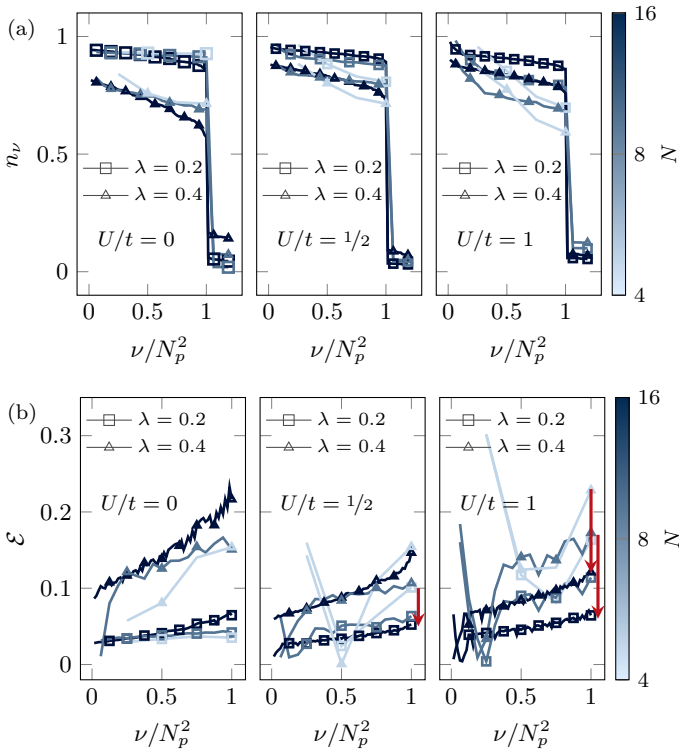


FIG. 2. In (a) the fragmentation of the 2RDM driven by strong correlations is illustrated. Increasing the particle number  $N$ , the formation of plateaus with occupation  $n_\nu \sim 1$ , composed of  $N_p^2 = (N/2)^2$  eigenvalues is observed for  $U/t > \lambda > 0$ . The eigenmodes  $\hat{\varphi}_\nu^\dagger$  associated with the plateaus are close to their maximal occupation, which is illustrated in (b), where we plot the deviation  $\mathcal{E}$  of the  $\hat{\varphi}_\nu^\dagger$ 's commutation relations from hardcore bosonic ones. The arrows indicate how the hardcore bosonic character of the  $\hat{\varphi}_\nu^\dagger$ 's evolves with increasing  $N$  and  $U$ .

this limit, we observe tightly bound bipolarons (shown in [40]), in agreement with the findings discussed in [9].

#### Maximally fragmented condensation at finite densities

We now turn to the question of correlation-driven electron pairing and condensation at finite filling fractions. For that purpose, we diagonalize the 2RDM's matrix elements  $\rho_{(ij),(mn)}$  yielding the representation of  $\hat{\rho}^{(2)}$  in terms of its eigenmodes  $\hat{\varphi}_\nu^{(\dagger)} = \sum_{ij} \bar{v}_{\nu,ij} \hat{c}_{i,\uparrow}^\dagger \hat{c}_{j,\downarrow}^\dagger$

$$\hat{\rho}^{(2)} = \sum_{\nu} n_{\nu} \hat{\varphi}_{\nu}^{\dagger} \hat{\varphi}_{\nu}, \quad (6)$$

with  $v_{\nu,ij}$  being the  $(ij)$ th component of the  $\nu$ th eigenvector of  $\rho_{(ij),(mn)}$ . The standard procedure to detect a superfluid or superconducting state, i.e., (quasi) off-diagonal long-range order (ODLRO), in the ground state is to check for the existence of a dominant eigenvalue  $n_{\nu_{\max}} \sim N^\alpha$  [52, 53] with  $N$  being the number of electrons in the system. The exponent  $\alpha$  is bounded to  $\alpha \leq 1/2$  in finite-range interacting, one-dimensional systems due to the Mermin-Wagner theorem [54, 55]. Besides the detection of ODLRO, recently the possible existence of

fragmented condensates has been suggested [23], a situation in which not only one but several eigenvalues acquire dominant behavior. In this case, it becomes crucial also to investigate the eigenvectors of  $\rho_{(ij),(mn)}$ , which can provide insights into the correlation structure of the ground-state wave function.

In Fig. 2a we show the largest eigenvalues  $n_\nu$  of the 2RDM in the ground state as a function  $\nu$  sorted in descending order, varying the filling  $N$  as well as both the electron-electron and electron-phonon interactions, for a system with  $L = 64$  lattice sites. For the  $U/t = 0$  case shown in the left panel, we observe a softening of the dominant eigenvalues when the filling is increased and, crucially, no evidence for an extensively scaling eigenvalue, i.e., no onset of condensation into one mode. This softening is a precursor for a model instability where we find that for  $\lambda = 0.5$  the model becomes unstable due to an unphysical change of the sign of hopping induced by large phonon distortions [39, 40]. Upon onset of this unphysical behavior, electrons form localized puddles of charge, i.e. "phase-separate", which translates into a wide distribution of two-particle states in momentum space and thus lead to the loss of the plateau-like structure in the 2RDM eigenvalues. The situation changes upon turning on the repulsive interactions as shown in the middle and right panels for the cases  $U/t = 0.5$  and  $U/t = 1$ , respectively. Here, with increasing the filling, we observe a flattening of the largest eigenvalues close to  $n_\nu = 1$ , which is stabilized up to larger values of  $\lambda$  and a sharp drop after the first  $(N/2)^2$  eigenvalues. We interpret this observation as the formation of a maximally fragmented condensate of two-particle bound states which we will justify in the following. We first note that given the form of the eigenmodes  $\hat{\varphi}_\nu^{(\dagger)}$ , there are  $(N/2)^2 \equiv N_p^2$  possible, orthogonal two-particle states. In order to rule out that the observation of exactly  $N_p^2$  eigenvalues of magnitude  $\sim 1$  is accidental, we calculate the commutation relations of the eigenmodes, which can be written as

$$\langle [\hat{\varphi}_\nu, \hat{\varphi}_{\nu'}^\dagger] \rangle = \delta_{\nu,\nu'} - \sum_{jlm,\sigma} \bar{v}_{\nu,jm} v_{\nu',lm} \langle \hat{c}_{j,\sigma} \hat{c}_{l,\sigma}^\dagger \rangle. \quad (7)$$

For bosonic commutation relations, the second contribution must vanish, which is a necessary condition for the existence of a conventional condensate. Since the observed occupations already indicate the absence of condensation, we evaluate the relative deviation from the hardcore bosonic case

$$\mathcal{E} = \frac{1}{2n_\nu} \left| \delta_{\nu,\nu'} (1 - 2n_\nu) - \langle [\hat{\varphi}_\nu, \hat{\varphi}_{\nu'}^\dagger] \rangle \right|, \quad (8)$$

shown in Fig. 2b. Increasing the repulsive on-site interaction  $U/t$ , we observe a strong tendency towards hardcore bosonic commutation relations, i.e.,  $\mathcal{E} \rightarrow 0$ , with increasing particle number, indicated by the arrows in the middle and right panels. Thus, the observed occupations of the 2RDM are close to their maximal value and in particular  $n_\nu > 1$  is impossible. Figure 2b suggests that in

this regime the 2RDM eigenmodes satisfy in the ground state the commutation relations

$$\langle [\hat{\varphi}_\nu, \hat{\varphi}_{\nu'}^\dagger] \rangle \approx \delta_{\nu,\nu'} \left( 1 - \langle \hat{n}_{\nu,\uparrow}^\varphi \rangle - \langle \hat{n}_{\nu,\downarrow}^\varphi \rangle \right), \quad (9)$$

where we introduced the density operator  $\hat{n}_{\nu,\sigma}^\varphi$  of the eigenmodes. The  $SU(2)$  symmetry of the SSH model suggests the identification  $n_\nu = \langle \hat{n}_{\nu,\uparrow}^\varphi \rangle = \langle \hat{n}_{\nu,\downarrow}^\varphi \rangle$ . As a consequence, we find that the 2RDM can be well-approximated by a mixed state

$$\hat{\rho}^{(2)} = \sum_{\nu=1}^{N_p^2} n_\nu |\varphi_\nu\rangle \langle \varphi_\nu| \quad (10)$$

where the two-particle states  $|\varphi_\nu\rangle$  describe hardcore bosons. Note that while the  $|\varphi_\nu\rangle$  can also be interpreted as composite bosons [56, 57], here the effective hardcore constraints occur in the space of the 2RDM's eigenmodes labeled by the mode-index  $\nu$ .

*Cooper-pairing at finite densities* A physical picture of the maximally fragmented condensate can be established by investigating the correlation structure in the two-particle states  $|\varphi_\nu\rangle$ . Taking a Fourier transformation with respect to the spin-up (index  $j$ ) and spin-down (index  $m$ ) components of the 2RDM's eigenstates  $v_{\nu,jm}$ , yields their momentum-space components  $v_\nu(k_\uparrow, k_\downarrow)$ . We find that the different eigenmodes  $|\varphi_\nu\rangle$  can be characterized by a finite momentum  $k_\nu$  and are dominated by contributions  $v_\nu(k_\uparrow, k_\downarrow) \approx v_\nu(k) \delta_{k_\downarrow, -k_\uparrow + k_\nu}$ :

$$|\varphi_\nu\rangle = \frac{1}{L} \sum_k v_\nu(k) \hat{c}_{\uparrow,k}^\dagger \hat{c}_{\downarrow,-k+k_\nu}^\dagger |\emptyset\rangle. \quad (11)$$

In general, we observe that the largest eigenvalue  $n_0$  has  $k_\nu = 0$ . This case is shown in Fig. 3a for  $N = 16$  using  $L = 64$  lattice sites. Upon increasing the repulsive interactions, the strong peak at  $k = 0$  is transformed into a plateau when  $U/t > \lambda > 0$ , decaying algebraically for  $k > k_F$ . This is reminiscent of Cooper-pairing and we further corroborate this observation by showing the phase factor of  $v_\nu(k)$  in the insets. In the BCS picture, the amplitudes of the two-particle states are related to the phase factor of the momentum dependent pairing gap

$$\Delta_k = |\Delta_k| e^{i\varphi_k} = |\Delta_k| e^{i \arg v_\nu(k)}. \quad (12)$$

Here, we can observe a characteristic jump from  $\arg v_\nu(k < k_F) = 0$  to  $\arg v_\nu(k > k_F) = \pi$ . Hence,  $\arg v_\nu(k) = \pi$  yields a momentum dependent pairing gap  $\Delta_{k > k_F} < 0$ , indicating a Cooper instability. This is supported by fitting the wave functions with the usual BCS-type ansatz for  $k > k_F$ :

$$v_\nu(k > k_F) = \mathcal{N} \sqrt{1 - \frac{\xi_k}{\sqrt{\xi_k^2 + \Delta^2}}}, \quad (13)$$

with  $\xi_k = -2t \cos(k) - \mu$  where  $\mu$  is the chemical potential, and  $\Delta$  the BCS gap. We find excellent agreement

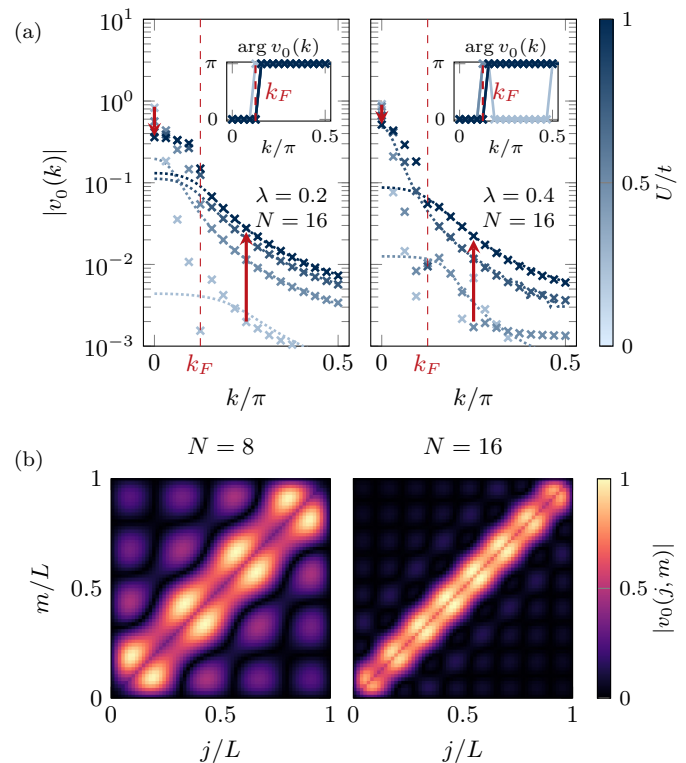


FIG. 3. Emergence of polaronic Cooper-pairing in the 2RDM eigenstate with  $\nu = 0$  corresponding to the largest eigenvalue. In the main plots of (a) the momentum-space components  $v_\nu(k_\uparrow, k_\downarrow)$  of the 2RDM's eigenmodes are shown along their dominant contributions  $k_\uparrow = -k_\downarrow \equiv k$ . Above the Fermi momentum  $k > k_F$  and in the strongly coupled regime  $U/t > \lambda > 0$  a Cooper-instability is inferred, where in the insets the phase of the BCS-pairing gap  $\Delta_k = v_0(k)$  is shown. The dotted lines in the main plots are obtained from fitting  $|v_0(k)|$  for momenta with  $\Delta_k < 0$ , using the BCS wave function. Real space components  $|v_{\nu,jm}|$  of the eigenmodes are shown in (b) in the strongly interacting regime  $U/t = 1.0$ ,  $\lambda = 0.4$ . A characteristic length scale  $\pi/k_F = \frac{2L}{N}$  of Cooper-pairing set by  $\Delta_k < 0$  if  $k > k_F$  is clearly visible in the form of non-overlapping areas of charge accumulation.

for the BCS-type ansatz applied to the 2RDM's eigenstates in the strong coupling regime  $U/t > \lambda > 0$ , shown in Fig. 3a as dotted lines. We emphasize that Cooper-pairing is restricted to a length scale set by  $a \sim 1/k_F$ . In real space, this translates into spatially non-overlapping, correlated areas of charge accumulations, each of which can be understood as region with dominant pairing correlations, as shown in Fig. 3b for the case  $L = 64$ ,  $U/t = 1$  and  $\lambda = 0.4$  at fillings  $N = 8$  and  $N = 16$ . Notably, for  $\nu > 0$  we always find finite-momentum Cooper pairing, which follows from the fact that the different eigenstates of the 2RDM have to be orthogonal but can not be populated with more than one pair of electrons (i.e., effective hardcore constraint).

*Discussion and Outlook* Our results have important consequences regarding the conventional picture of bipolaronic superconductivity in the adiabatic limit. We

demonstrated that for the one-dimensional SSH-model, molecular bipolarons are unstable in the physically relevant regime. Our analysis of the 2RDM indicates that at strong interactions  $U/t > \lambda > 0$ , polarons form pairs with a large spatial coherence length, reminiscent of Cooper pairing. Therefore, the ground state at finite filling fractions is not a superfluid of molecular bipolarons, but rather a strongly correlated mixture of bipolaron-like polaronic pairs with finite momenta in a state, characterized as a maximally fragmented condensate. We also point out that at finite fillings, the interplay between strong repulsive interactions and comparably weak electron-phonon couplings is what yields the most pronounced pairing, a setting that is more typical of actual physical systems. A possible physical mechanism behind these findings may be a tendency of the off-diagonal electron-phonon coupling to generate pair-density wave correlations. In fact, there is recent evidence that such density fluctuations could generate fragmentation [24], an avenue we plan to explore in future work. These results call for further unbiased investigations of the phase diagram of electron-phonon systems with off-diagonal coupling in order to establish possible pairing mechanisms in physically realistic systems.

## ACKNOWLEDGMENTS

We thank Alexander Wietek for inspiring discussions and Lode Pollet, Mona Berciu and Andrew Millis for comments on the manuscript. M. G., T. B., U. S. and S. P. acknowledge support by the Deutsche Forschungsgemeinschaft (DFG, German Research Foundation) under Germany's Excellence Strategy-426 EXC-2111-390814868. J. S. acknowledges support from the Gordon and Betty Moore Foundation's EPiQS Initiative through Grant GBMF8686 at Stanford University.

## Appendix A: Singlon-Doublon decomposition

In order to analyze the quasi-particles of the SSH model [58], it is convenient to represent the Hamiltonian in terms of momentum space operators. For that purpose, we introduce the Fourier transformed electronic spin- $\sigma$   $\hat{c}_{k,\sigma}^{(\dagger)}$  and  $\hat{a}_k^{(\dagger)}$  annihilation (creation) operators

$$\hat{c}_{k_n,\sigma} = \frac{1}{\sqrt{L}} \sum_j e^{-ik_n r_j} \hat{c}_{j,\sigma}, \quad (\text{A1})$$

$$\hat{a}_{k_n} = \frac{1}{\sqrt{L}} \sum_j e^{-ik_n r_j} \hat{a}_j, \quad (\text{A2})$$

where  $r_j = j \cdot a$  denotes the position of the  $j$ th lattice site and  $a$  is the lattice constant. Here, the discrete momenta  $k_n$  are elements of the Brillouin zone  $k_n = \frac{\pi}{L}n$  with  $n = -L, -L+1, \dots, L-1$ . For notational convenience we

drop the discrete index  $n$ :  $k_n \rightarrow k$  and implicitly perform summations over momentum space indices  $k, q$  with respect to their allowed ranges depending on the number of lattice sites  $L$ . The momentum space representation of the phononic displacement operator  $\sqrt{2M\Omega}\hat{X}_j = \hat{a}_j^\dagger + \hat{a}_j$  with the oscillator mass  $M$  can then be expressed as

$$\hat{X}_k = \frac{1}{L} \sum_j e^{-ikr_j} \hat{X}_j, \quad (\text{A3})$$

which satisfies  $\hat{X}_k^\dagger = \hat{X}_{-k}$ , and we set  $M \equiv 1$ . Considering  $U = 0$  for brevity, the SSH-model Hamiltonian in momentum space is given by

$$\hat{H} = - \sum_{k,\sigma} \varepsilon_k \hat{c}_{k,\sigma}^\dagger \hat{c}_{k,\sigma} + \Omega \sum_k \hat{a}_k^\dagger \hat{a}_k - \sum_{k,\sigma} \sum_q \left( V_{k,k-q} \hat{c}_{k,\sigma}^\dagger \hat{c}_{k-q,\sigma} \hat{X}_q + \text{h.c.} \right), \quad (\text{A4})$$

where we introduced  $\varepsilon_k = 2t \cos(k) - \mu$  and the Fourier-transformed electron-phonon coupling

$$V_{k,q} = i\alpha \sqrt{\frac{2\Omega}{L}} (\sin(k) - \sin(q)). \quad (\text{A5})$$

Note that for brevity the chemical potential  $\mu$  has been suppressed in the main text.

We now introduce strictly single- and two-particle electronic operators

$$\hat{s}_{j,\sigma}^{(\dagger)} = \left[ \hat{c}_{j,\sigma} (1 - \hat{n}_{j,\bar{\sigma}}^\dagger) \right]^{(\dagger)}, \quad (\text{A6})$$

$$\hat{d}_j^{(\dagger)} = \left[ \hat{c}_{j,\downarrow} \hat{c}_{j,\uparrow} \right]^{(\dagger)}, \quad (\text{A7})$$

where we defined the spin- $\sigma$  density operators  $\hat{n}_{j,\sigma} = \hat{c}_{j,\sigma}^\dagger \hat{c}_{j,\sigma}$  and denoted spin conjugation by an overbar

$$\bar{\sigma} = \begin{cases} \downarrow, & \text{if } \sigma = \uparrow, \\ \uparrow, & \text{if } \sigma = \downarrow. \end{cases} \quad (\text{A8})$$

These operators obey (anti-) commutation relations

$$\left\{ \hat{s}_{j,\sigma}, \hat{s}_{j',\sigma'} \right\} = 0, \quad \text{and} \quad \left[ \hat{d}_j, \hat{d}_{j'} \right] = 0, \quad (\text{A9})$$

as well as

$$\left\{ \hat{s}_{j,\sigma}, \hat{s}_{j',\sigma'}^\dagger \right\} = \delta_{j,j'} \delta_{\sigma,\sigma'} (1 - \hat{n}_{j,\bar{\sigma}}) \quad (\text{A10})$$

$$\left[ \hat{d}_j, \hat{d}_{j'}^\dagger \right] = \delta_{j,j'} e^{i\pi \hat{n}_j^d}, \quad (\text{A11})$$

with  $\hat{n}_j^d = \hat{d}_j^\dagger \hat{d}_j$ . Their Fourier representation is defined via

$$\hat{s}_{k,\sigma} = \frac{1}{\sqrt{L}} \sum_j e^{-ikr_j} \hat{s}_{j,\sigma}, \quad (\text{A12})$$

$$\hat{d}_k = \frac{1}{\sqrt{L}} \sum_j e^{-ikr_j} \hat{d}_j. \quad (\text{A13})$$

Finally, the inverse representation in terms of electronic operators is given by

$$\hat{c}_{j,\sigma} = \hat{s}_{j,\sigma} + \text{sgn}(\sigma) \hat{s}_{j,\bar{\sigma}}^\dagger \hat{d}_j, \quad (\text{A14})$$

$$\hat{c}_{j,\sigma}^\dagger = \hat{s}_{j,\sigma}^\dagger + \text{sgn}(\sigma) \hat{d}_j^\dagger \hat{s}_{j,\bar{\sigma}}, \quad (\text{A15})$$

$$\sum_{k,\sigma} \varepsilon_k \hat{c}_{k,\sigma}^\dagger \hat{c}_{k,\sigma} = \sum_{k,\sigma} \varepsilon_k \left\{ \hat{s}_{k,\sigma}^\dagger \hat{s}_{k,\sigma} + \hat{D}_{k,\sigma}^\dagger \hat{D}_{k,\sigma} + \text{sgn}(\sigma) \left( \hat{s}_{k,\sigma}^\dagger \hat{D}_{k,\sigma} + \text{h.c.} \right) \right\} \quad (\text{A18})$$

$$\sum_{\sigma} \sum_{k,q} V_{k,k-q} \hat{c}_{k,\sigma}^\dagger \hat{c}_{k-q,\sigma} \hat{X}_q = \sum_{k,\sigma} \sum_q V_{k,k-q} \left\{ \hat{s}_{k,\sigma}^\dagger \hat{s}_{k-q,\sigma} + \hat{D}_{k,\sigma}^\dagger \hat{D}_{k-q,\sigma} + \text{sgn}(\sigma) \left( \hat{s}_{k,\sigma}^\dagger \hat{D}_{k-q,\sigma} + \text{h.c.} \right) \right\} \hat{X}_q. \quad (\text{A19})$$

Let us briefly comment on the different operators and terms. The operators  $\hat{s}_{k,\sigma}^{(\dagger)}$  describe spin- $\sigma$  fermions (singlons) that are composed of a superposition of spin- $\sigma$  electrons, in which the electron solely occupies the lattice site, i.e., there are no double occupancies. Conversely, the operators  $\hat{d}_k^{(\dagger)}$  describe a superposition of hardcore bosons composed of electronic double occupancies (doublons). Let us now assume that there are stable on-site bipolarons, glued together by the electron-phonon interaction. Apparently, these bipolarons are then described by doublons dressed with phonons and if there are electrons that are not bound into on-site bipolarons, they must be described by singlons. The bilinear contributions  $\sum_{\sigma} \hat{D}_{k,\sigma}^\dagger \hat{D}_{q,\sigma} \equiv \hat{D}_k \hat{D}_q$  describe scattering processes between doublons and singlons where the total numbers of both species

$$\hat{N}_{s,\sigma} = \sum_j \hat{s}_{j,\sigma}^\dagger \hat{s}_{j,\sigma}, \quad \hat{N}_d = \sum_j \hat{d}_j^\dagger \hat{d}_j \quad (\text{A20})$$

are conserved. Finally, there are processes  $\hat{s}_{k,\sigma}^\dagger \hat{D}_{q,\sigma}$  and  $\hat{D}_{k,\sigma}^\dagger \hat{s}_{q,\sigma}$  converting doublons into singlons and vice versa, assisted by the annihilation/creation of an additional singlon with opposite spin  $\bar{\sigma}$ .

$$\begin{aligned} \text{el} \langle \hat{d}_k \hat{H}_{D-D} \hat{d}_{k'}^\dagger | \emptyset \rangle_{\text{el}} &= \frac{2}{L} \left\{ \delta_{k,k'} \sum_q \varepsilon_q + \sum_q \left( V_{q,q-(k-k')} \hat{X}_{k-k'} + \text{h.c.} \right) \right\} + \Omega \sum_q \hat{a}_q^\dagger \hat{a}_q + U \\ &\stackrel{L \rightarrow \infty}{\equiv} 2\mu \delta_{k,k'} + \frac{1}{\pi} \left( \hat{X}_{k-k'} - \hat{X}_{k-k'}^\dagger \right) \int_0^{2\pi} V_{q,q-(k-k')} dq + \Omega \hat{N}_a + U, \end{aligned} \quad (\text{B3})$$

with the total phonon number  $\hat{N}_a$ . The  $q$ -integral over the electron-phonon interaction vanishes, which follows immediately from Eq. (A5) where we can integrate both summands independently. Since  $\langle \hat{N}_a \rangle \geq 0$  it fol-

and their Fourier expansion is expressed as

$$\hat{c}_{k,\sigma} = \hat{s}_{k,\sigma} + \frac{\text{sgn}(\sigma)}{\sqrt{L}} \sum_q \hat{s}_{q-k,\bar{\sigma}}^\dagger \hat{d}_q, \quad (\text{A16})$$

$$\hat{c}_{k,\sigma}^\dagger = \hat{s}_{k,\sigma}^\dagger + \frac{\text{sgn}(\sigma)}{\sqrt{L}} \sum_q \hat{d}_q^\dagger \hat{s}_{q-k,\bar{\sigma}}. \quad (\text{A17})$$

Using these definitions as well as  $\hat{D}_{k,\sigma} = \frac{1}{\sqrt{L}} \sum_q \hat{s}_{q-k,\bar{\sigma}}^\dagger \hat{d}_q$ , the SSH-model can be decomposed into strictly single- and two-particle terms and contributions  $\propto \hat{D}_{k,\sigma}^{(\dagger)}$  that describe scattering processes between them. We obtain the decompositions

## Appendix B: Instability of on-site bipolarons

From the decomposition in App. A we can analyze the stability of an on-site bipolaron, described by dressed doublons. In the  $N = 2$  particle sector with total spin  $S^z = 0$ , if there is such a stable quasi particle, the eigenstates have the form

$$|\psi_k^d\rangle = \sum_q \psi_k^d(q) \hat{d}_q^\dagger |\emptyset\rangle_{\text{el}} |a_k(q)\rangle_{\text{ph}} \quad (\text{B1})$$

where  $|\emptyset\rangle$  is the electronic vacuum,  $|a_k(q)\rangle$  a phonon configuration characterized by the momenta  $k$  and  $q$  and  $\psi_k^d(q) \in \mathbb{C}$ . For this ansatz to be an eigenstate, all matrix elements describing pure singlons and singlon-doublon conversion must vanish such that it suffices to consider only the matrix elements of the Hamiltonian containing bilinear contributions  $\hat{D}_k \hat{D}_q$ :

$$\hat{H}_{D-D} = \sum_k \left( \varepsilon_k \hat{D}_k^\dagger \hat{D}_k + \sum_q \left( V_{k,k-q} \hat{D}_k^\dagger \hat{D}_{k-q} \hat{X}_q + \text{h.c.} \right) \right). \quad (\text{B2})$$

Calculating the matrix elements w.r.t. the electronic states we find

lows that eigenvalues  $E_k^d$  belonging to eigenstates of the form Eq. (B1), if existant at all, satisfy  $E_k^d \geq \mu + U$ . Hence, there are no bound on-site bipolaron states in the two-particle sector, i.e., bipolaronic bound states must be

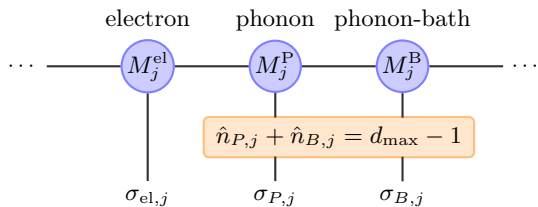


FIG. 4. Decomposition of the unit cell, containing an electronic degree of freedom  $|\sigma_{el,j}\rangle$ , a phononic degree of freedom  $|\sigma_{P,j}\rangle$  and the corresponding phononic bath site  $|\sigma_{B,j}\rangle$ . The PP gauge constraint is indicated as two-site gate, which, in practice, is absorbed into the construction of the Hamiltonian [21]

delocalized over at least two lattice sites. In the bipolaronic spectral function we indeed observe these states as incoherent signal at energies  $\omega \sim \Omega + U$  which is consistent with the choice  $\mu = 0$  for our calculations. However, this band exhibits a small dispersion that can be addressed to scatterings into polarons, which we neglected in the above calculation.

### Appendix C: Projected purified matrix-product states

One of the main advantageous of tensor-network state (TNS)-based techniques is their capability to provide a controlled approximation of the total many-body wavefunction. For the case of matrix-product states (MPS), this representation is obtained from an ansatz class for the wavefunction's coefficients of the form

$$c_{\sigma_1, \dots, \sigma_L} = \sum_{\sigma_1, \dots, \sigma_L} M^{\sigma_1} \dots M^{\sigma_L} |\sigma_1, \dots, \sigma_L\rangle, \quad (\text{C1})$$

where the  $\sigma_j = 0, \dots, d_j - 1$  denote the  $L \in \mathbb{N}$  local degrees of freedom, spanning the overall many-body Hilbert space, and  $M^{\sigma_j} \in \mathbb{C}^{m_{j-1} \times m_j}$  are complex matrices with bond dimensions  $m_j$ , encoding the wavefunction. For systems with small local Hilbert space dimensions  $d_j$ , there are efficient contraction and compression schemes but the situation changes drastically, if some of the local degrees of freedoms describe harmonic oscillators where in principle  $d_j = \infty$ . In that cases one typically introduces a finite cutoff dimension  $d_{\max}$ , which, however must be chosen carefully such that the physical properties are not affected by the artificial truncation. Clearly, selecting a proper value  $d_{\max}$  depends on the particular basis chosen to represent the bosonic modes and different ways have been explored in the past [20, 21, 59, 60]. In this work, we use projected purified matrix-product states (PP-MPS) which allow for a dynamical adoption of the number of actually used local basis states  $d_{\text{eff}} \leq d_{\max}$ , given a suitably large value of  $d_{\max}$ . The key idea is to introduce for each bosonic lattice site  $|\sigma_{P,j}\rangle$  an artificial bath site  $|\sigma_{B,j}\rangle$  that acts as reservoir for the physical

bosonic excitations, such that for each pair of physical and bath site, the overall number of bosonic excitations is conserved:  $\hat{n}_{P,j} + \hat{n}_{B,j} = d_{\max} - 1$ . This gauge constraint introduces a global  $U(1)$ -symmetry for the bosonic degrees of freedom, allowing for a drastic reduction of the numerical complexity, in particular if parallelization is exploited [21, 61]. Furthermore, it can be shown that for a bipartition of the overall system between bosonic physical and bath sites, the Schmidt values can be identified with the bosonic excitation probabilities, allowing for a controlled truncation of irrelevant bosonic basis states.

### Appendix D: Time Evolution Methods

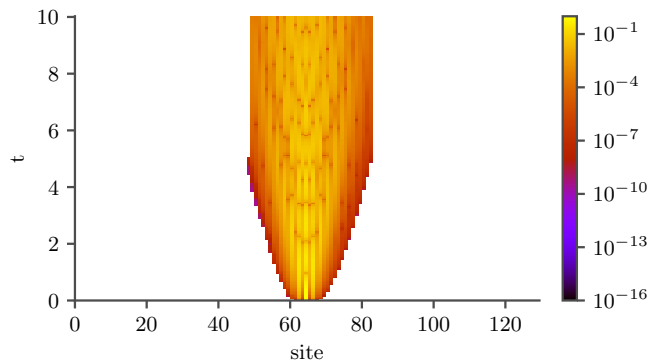


FIG. 5. Light cone for an electronic excitation at  $\Omega = 0.4$  and  $\lambda = 0.5$  using GSE and 2TDVP.

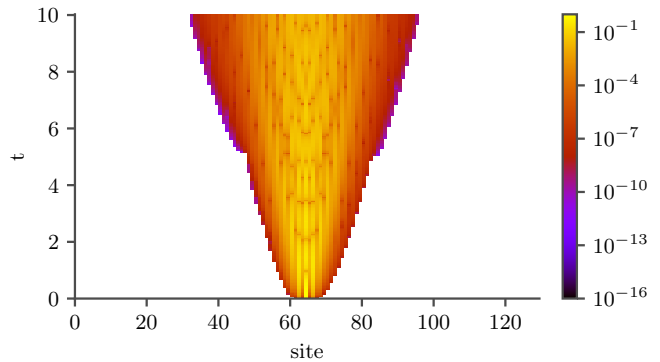


FIG. 6. Light cone for an electronic excitation at  $\Omega = 0.4$  and  $\lambda = 0.5$  using GSE and LSE.

Due to their unfavourable scaling in the local dimension of our Hilbert space, the commonly used TNS time evolution methods [17] time-dependent variational principle (TDVP), in its two-site variant, [62, 63] or time-evolving block-decimation (TEBD) [64–66] perform notoriously poor for the simulation of electron-phonon systems. Recent developments brought forth subspace expansion extensions for single-site time-dependent variational principle (1TDVP) that scale with  $d^2$  instead of  $d^3$ ,

whilst still conserving the ability to dynamically grow the bond dimension[18, 19]. The GSE builds a small Krylov subspace of typically 3 – 5 Krylov vectors that can be used to enrich the state. As the construction of these Krylov Vectors is rather expensive, we resort to the LSE for most of our calculation. LSE aims to enrich the state with a local expansion tensor. We are using the expansion scheme introduced by Hubig et al. [67]:

$$E_i = L_{i-1}M_iW_i \quad (D1)$$

where  $L_{i-1}$  are the left contractions,  $M_i$  is the active site tensor and  $W_i$  the corresponding MPO. The contractions can be build iteratively during a TDVP sweep,  $L_i = L_{i-1}A_i^\dagger W_i A_i$  with  $L_0 = 1$ . It not only scales better than 2TDVP in the local dimension it is also more stable in regards to small bond dimensions [17, 19]. This is crucial for our calculations as we are calculating the dynamics of excitations on a product state. Figure 5 shows the light cone of an electronic excitation at  $\Omega = 0.4$  simulated using 2TDVP. As we can see, the expansion of the light cone freezes and the excitation is trapped in a system of finite size. LSE, however, manages to accurately continue spread theof the excitation.

### Local Subspace Expansion - LSE

In the following we will give a step wise description of a left-to-right MPS sweep of the LSE. The update scheme of the  $i$ th site tensor is[19]:

1. time evolve the site tensor  $M_i(t) \rightarrow M_i(t + \frac{\delta t}{2})$
2. truncate the site tensor  $M_i$  using a SVD and obtain the decomposition  $M_i = B_i S_i A_i$ .
3. evaluate heuristically whether to expand, renormalize  $S_i$  and build bond tensor  $D_i = S_i A_i$ 
  - (a) if no expansion is needed update site tensor  $M_i = B_i$ ; jump to step 9
  - (b) else, build the projector onto the orthogonal compliment of  $M_i$ ,  $P_i = \mathbb{1} - B_i B_i^\dagger$
4. build the expansion tensor  $E_i = \alpha_i L_{i-1} M_i W_i$
5. project it onto the orthogonal compliment  $E_i^\perp = E_i P_i$ 
  - (a) if the norm is of  $E_i^\perp$  is zero, update site tensor  $M_i = B_i$ ; jump to step 9
  - (b) else, truncate the expansion tensor and obtain the decomposition  $E_i^\perp = B_i^\perp S_i^\perp A_i^\perp$
6. enlarge  $B_i$  via direct sum as  $\tilde{B}_i = [B_i \ B_i^\perp]$
7. build new expanded bond tensor via  $D_i = \tilde{B}_i^\dagger M_i$
8. calculate new left contractions  $L_i = L_{i-1} A_i^\dagger W_i A_i$

9. back evolve bond tensor  $D_i(t + \frac{\delta t}{2}) \rightarrow D_i(t)$

10. multiply  $D_i$  into the next site tensor  $B_{i+1}$

A further advantage of this method over 2TDVP is, that it is not plagued by stability issues at small bond dimensions[17]. This turns out to be crucial for our simulations as we are calculating the dynamics of an excitation on a product state. As shown in Fig. 5, 2TDVP fails to accurately describe the spread of the excitation after we switch the time evolution method from GSE to 2TDVP at  $T = 5$ .

### Extracting (Bi-)Polaronic Dispersion Relation from Spectral Functions

We calculated the time-dependent, (bi-)polaron Greens functions

$$G_P(j, t) = \langle \emptyset | \hat{c}_{j,\sigma}(t) \hat{c}_{L/2,\sigma}^\dagger(0) | \emptyset \rangle \quad \text{polaron}, \quad (D2)$$

$$G_{BP}(j, t) = \langle \emptyset | \hat{d}_j(t) \hat{d}_{L/2}^\dagger(0) | \emptyset \rangle \quad \text{bipolaron}, \quad (D3)$$

where  $|\emptyset\rangle$  denotes the combined electron-phonon vacuum state,  $\hat{c}_{j,\sigma}^{(\dagger)}$  are spin- $\sigma$  electronic annihilation (creation) operators and  $\hat{d}_j^{(\dagger)} = \hat{c}_{j,\uparrow}^\dagger \hat{c}_{j,\downarrow}$ . Taking two Fourier transformations then yields the momentum resolved spectral functions (with  $\alpha = \text{P, BP}$ )

$$S_\alpha(k, \omega) = \frac{\pi}{T\sqrt{L}} \sum_{j,n} e^{-i(k \cdot j - \omega \cdot t_n) - \eta t_n} G_\alpha(j, t_n), \quad (D4)$$

where the  $j$ -sum is over all lattice sites. In Fig. 7 we show momentum cuts of the obtained (bi-)polaronic spectral functions, exemplarily. The dispersion relation is then extracted by determining the position of the low-energy peaks (indicated as dots)  $\varepsilon_{\text{P/BP}}(k)$ . We fit their positions around their minimum value  $\varepsilon_{\text{P/BP}}^0$  using a quadratic ansatz

$$\varepsilon_{\text{P/BP}}(k) = \varepsilon_{\text{P/BP}}^0 + \frac{k^2}{2m_{\text{eff}}}, \quad (D5)$$

with the quasi-particle effective mass  $m_{\text{eff}} = \left. \frac{\partial^2 E}{\partial k^2} \right|_{k=0}$ . For the considered couplings in the adiabatic limit, we always find  $\varepsilon_{\text{P/BP}}^0$  to be located at  $k = 0$  for both, polarons (P) and bipolarons (BP).

Previous works already studied the properties of bipolaronic quasi-particles in the anti-adiabatic regime. In order to connect to these investigations, in Fig. 7c we show the bipolaronic binding energies  $\Delta_{\text{BP}}(k = 0) = \varepsilon_{\text{BP}}(0) - 2\varepsilon_{\text{P}}(0)$  at larger phonon frequencies  $\Omega/t = 1$ . The observation of tightly bound bipolarons with binding energies whose absolute value increases with the effective electron-phonon coupling is in perfect agreement with previous findings [9].

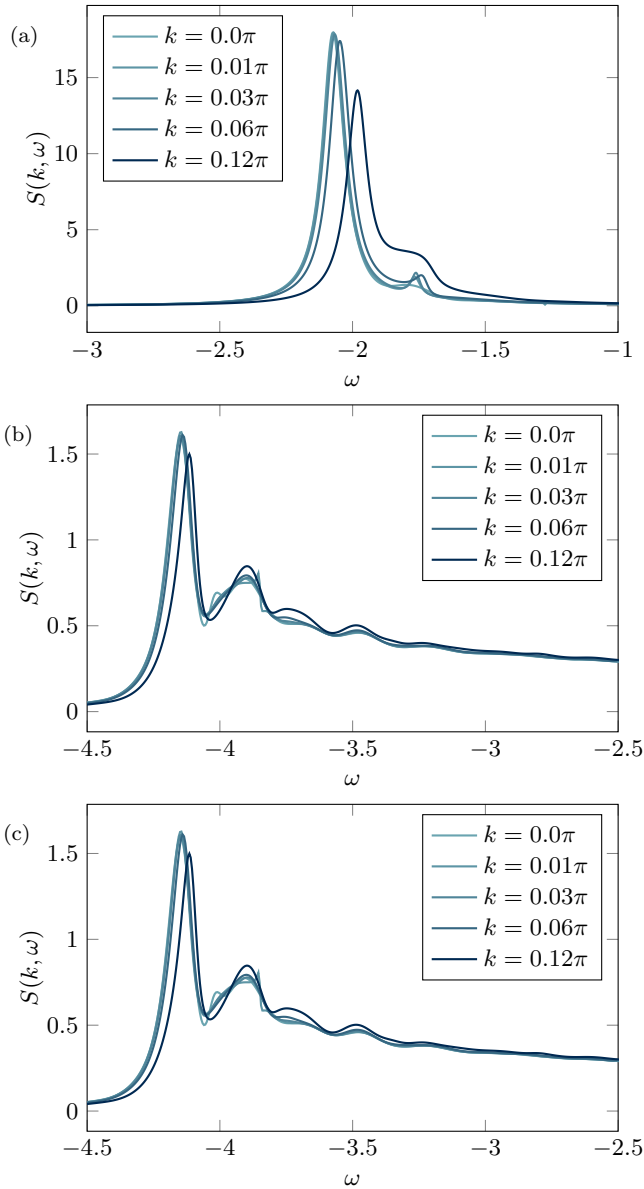


FIG. 7. Momentum cuts of spectral functions calculated for  $U/t = 0$  and  $\lambda = 1/2$ . The polaron spectral functions are shown in (a), the bipolaronic spectral functions in (b). Dots are indicating the position of the maximum of the energetically lowest peak, from which the polaronic/bipolaronic dispersion relation is reconstructed. In (c), the bipolaronic binding energy at larger phonon frequencies  $\Omega/t = 1$  is shown. Previous investigations already reported the formation of bipolarons in the anti-adiabatic regime, which is confirmed by our observations of large bipolaronic binding energies  $|\Delta_{BP}(k=0)/t|$ .

### Appendix E: Ground-state results in the low-density limit

In order to supplement our findings we performed ground-state calculations for the SSH-model in the dilute limit  $n = N/2L < 0.1$ . In the adiabatic limit, these

calculations are challenging due to low energy costs to create phononic excitations. For that purpose we chose a large number of maximally allowed local phononic excitations  $n_{\text{ph,max}} = 63$  which we found to ensure convergence also for the largest systems studied, with up to  $L = 256$  lattice sites. For the maximally allowed truncated weight we chose  $\delta = 10^{-10}$ , for which a maximum bond dimension of  $m = 2048$  states was sufficient. Using both, single- and two-site MPS solvers [67] we converged the ground-state calculations to a relative precision of  $\Delta E_0/E_0 = 10^{-8}$  where  $\Delta E_0$  denotes the change in the ground-state energy  $E_0$  in the last sweep. However, these parameters need to be taken with a grain of salt, since the SSH-model can become unstable in certain parameter regimes, as discussed below. Once that unphysical regime is entered, phase separation sets in, generating a large number of excited states that are energetically located very close above the ground state. In that situation, and using open boundary conditions, the simulations are prone to get stuck in such local minima, which we diagnosed by investigating either the symmetry of local observables such as the electron density, or the (staggered) phonon displacements.

### Stability of the SSH-Model at Strong Electron-Phonon Couplings

In the SSH model, the electron-phonon coupling is assumed to be strongly suppressed at equilibrium lattice distances  $|i - j| > 1$  and therefore neglected. This approximation can cause unphysical behavior that is reflected in a sign-change of the electron hopping and signalled by displacements  $-\langle \hat{X}_j \rangle - \langle \hat{X}_{j+1} \rangle > 1$ , i.e., displacements are so large that the atomic coordinates are moved across each other [38]. Note that in previous studies, due to numerical limitations, even in the non-adiabatic regime, this unphysical behavior was regularized by introducing a rather sharp cutoff in the maximally allowed number of phononic excitations per site [38]. While this can be justified at large phonon frequencies  $\Omega \sim t$ , in the adiabatic limit we observe very large numbers of  $\sim 30$  excitations per lattice site, which are automatically chosen by the truncation scheme of our projected purified density-matrix renormalization group (PP-DMRG) solver, and are numerically controlled w.r.t. the truncated weight [20, 21].

In order to check our results for physical consistency, we performed ground-state calculations and monitored the maximally occurring staggered displacements

$$\Delta X_{\text{max}} = \max_{j \in [0, L-1]} \left( \langle \hat{X}_j \rangle - \langle \hat{X}_{j+1} \rangle \right). \quad (\text{E1})$$

Results are shown exemplary for the cases  $U/t = 0$  in Fig. 8a and  $U/t = 1/4$  in Fig. 8b. For the considered electron-phonon coupling ranges  $\lambda \in [0, 1/2]$ , we observed instabilities only in case of vanishing electron-electron

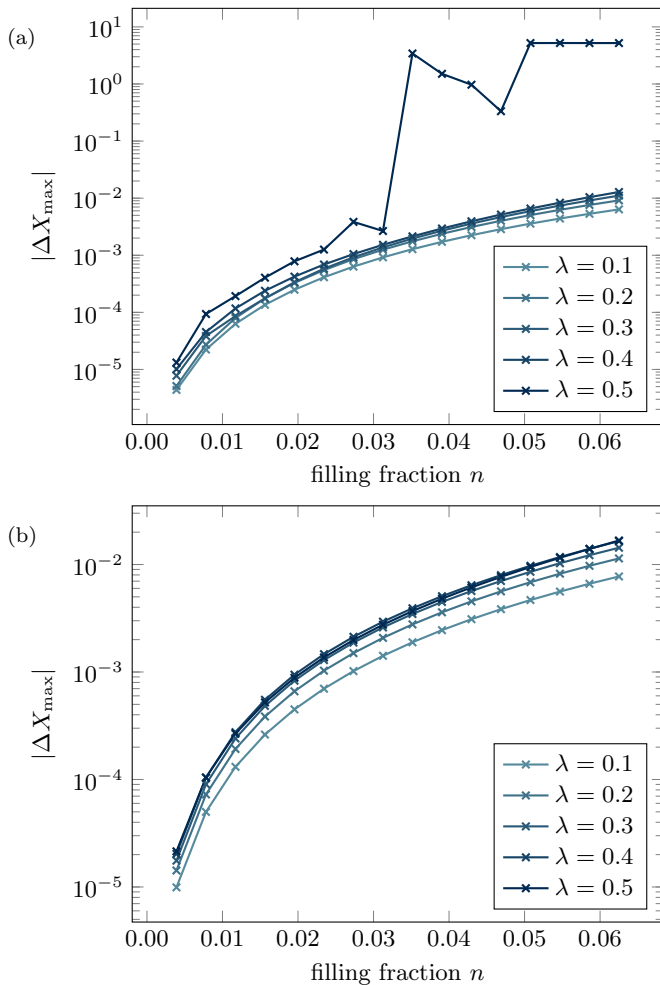


FIG. 8. Minimally observed staggered magnetization  $\Delta X_{\max} = \max_{j \in [0, L-1]} (\langle \hat{X}_j \rangle - \langle \hat{X}_{j+1} \rangle)$  as a function of the filling fraction  $n = N/L$  and the electron-phonon coupling  $\lambda$ . Values  $|\Delta X_{\max}| > 1$  are indicating lattice instabilities and thus a breakdown of the physicality of the SSH model. We show exemplary results for  $U/t = 0$  in (a) and  $U/t = 1/4$  in (b) for a system size of  $L = 256$ .

interactions and for filling fractions  $n > 0.025$ , at the largest coupling strength  $\lambda = 1/2$ .

- 
- [1] H. Fröhlich, H. Pelzer, and S. Zienau, Xx. properties of slow electrons in polar materials, *The London, Edinburgh, and Dublin Philosophical Magazine and Journal of Science* **41**, 221 (1950), <https://doi.org/10.1080/14786445008521794>.
- [2] H. Fröhlich, Electrons in lattice fields, *Advances in Physics* **3**, 325 (1954), <https://doi.org/10.1080/00018735400101213>.
- [3] T. Holstein, Studies of polaron motion: Part i. the molecular-crystal model, *Annals of Physics* **281**, 706 (2000).
- [4] T. Holstein, Studies of polaron motion: Part ii. the “small” polaron, *Annals of Physics* **281**, 725 (2000).
- [5] A. Alexandrov and J. Ranninger, Theory of bipolarons and bipolaronic bands, *Phys. Rev. B* **23**, 1796 (1981).
- [6] A. Alexandrov and J. Ranninger, Bipolaronic superconductivity, *Phys. Rev. B* **24**, 1164 (1981).
- [7] A. S. Alexandrov, J. Ranninger, and S. Robaszkiewicz, Bipolaronic superconductivity: Thermodynamics, magnetic properties, and possibility of existence in real substances, *Phys. Rev. B* **33**, 4526 (1986).
- [8] B. K. Chakraverty, J. Ranninger, and D. Feinberg, Experimental and theoretical constraints of bipolaronic superconductivity in high  $T_c$  materials: An impossibility, *Phys. Rev. Lett.* **81**, 433 (1998).
- [9] J. Sous, M. Chakraborty, R. V. Krems, and M. Berciu, Light bipolarons stabilized by peierls electron-phonon coupling, *Phys. Rev. Lett.* **121**, 247001 (2018).

- [10] M. R. Carbone, A. J. Millis, D. R. Reichman, and J. Sous, Bond-peierls polaron: Moderate mass enhancement and current-carrying ground state, *Phys. Rev. B* **104**, L140307 (2021).
- [11] J. Sous, Y. He, and S. A. Kivelson, [Absence of a bcs-bec crossover in the cuprate superconductors](#) (2022).
- [12] A. T. Ly, B. Cohen-Stead, S. M. Costa, and S. Johnston, A comparative study of the superconductivity in the holstein and optical su-schrieffer-heeger models (2023), [arXiv:2307.10809 \[cond-mat.supr-con\]](#).
- [13] K.-S. Kim, Z. Han, and J. Sous, Semi-classical theory of bipolaronic superconductivity in a bond-modulated electron-phonon model (2023), [arXiv:2308.01961 \[cond-mat.supr-con\]](#).
- [14] C. Zhang, J. Sous, D. Reichman, M. Berciu, A. Millis, N. Prokof'ev, and B. Svistunov, Bipolaronic high-temperature superconductivity, *Physical Review X* **13**, 10.1103/physrevx.13.011010 (2023).
- [15] X. Cai, Z.-X. Li, and H. Yao, High-temperature superconductivity induced by the su-schrieffer-heeger electron-phonon coupling (2023), [arXiv:2308.06222 \[cond-mat.str-el\]](#).
- [16] U. Schollwöck, The density-matrix renormalization group in the age of matrix product states, *Annals of Physics* **326**, 96 (2011), january 2011 Special Issue.
- [17] S. Paeckel, T. Köhler, A. Swoboda, S. R. Manmana, U. Schollwöck, and C. Hubig, Time-evolution methods for matrix-product states, *Annals of Physics* **411**, 167998 (2019).
- [18] M. Yang and S. R. White, Time-dependent variational principle with ancillary krylov subspace, *Physical Review B* **102**, 10.1103/physrevb.102.094315 (2020).
- [19] M. Yang and S. R. White, [Time dependent variational principle with ancillary krylov subspace](#) (2020).
- [20] T. Köhler, J. Stolpp, and S. Paeckel, Efficient and flexible approach to simulate low-dimensional quantum lattice models with large local Hilbert spaces, *SciPost Phys.* **10**, 058 (2021).
- [21] J. Stolpp, T. Köhler, S. R. Manmana, E. Jeckelmann, F. Heidrich-Meisner, and S. Paeckel, Comparative study of state-of-the-art matrix-product-state methods for lattice models with large local hilbert spaces without u(1) symmetry, *Computer Physics Communications* **269**, 108106 (2021).
- [22] E. J. Mueller, T.-L. Ho, M. Ueda, and G. Baym, Fragmentation of Bose-Einstein condensates, *Physical Review A* **74**, 10.1103/physreva.74.033612 (2006).
- [23] A. Wietek, Fragmented cooper pair condensation in striped superconductors, *Phys. Rev. Lett.* **129**, 177001 (2022).
- [24] N. Baldelli, B. Kloss, M. Fishman, and A. Wietek, Fragmented superconductivity in the hubbard model as solitons in ginzburg-landau theory (2023), [arXiv:2307.11820 \[cond-mat.str-el\]](#).
- [25] M. Weber, F. F. Assaad, and M. Hohenadler, Excitation spectra and correlation functions of quantum su-schrieffer-heeger models, *Physical Review B* **91**, 10.1103/physrevb.91.245147 (2015).
- [26] M. Weber, F. F. Assaad, and M. Hohenadler, Continuous-time quantum Monte Carlo for fermion-boson lattice models: Improved bosonic estimators and application to the Holstein model, *Phys. Rev. B* **94**, 245138 (2016).
- [27] M. Weber, F. F. Assaad, and M. Hohenadler, Directed-loop quantum monte carlo method for retarded interactions, *Phys. Rev. Lett.* **119**, 097401 (2017).
- [28] T. Shi, E. Demler, and J. Ignacio Cirac, Variational study of fermionic and bosonic systems with non-gaussian states: Theory and applications, *Annals of Physics* **390**, 245 (2018).
- [29] M. Weber, F. Parisen Toldin, and M. Hohenadler, Competing orders and unconventional criticality in the Su-Schrieffer-Heeger model, *Phys. Rev. Res.* **2**, 023013 (2020).
- [30] D. Jansen, J. Bonča, and F. Heidrich-Meisner, Finite-temperature density-matrix renormalization group method for electron-phonon systems: Thermodynamics and holstein-polaron spectral functions, *Phys. Rev. B* **102**, 165155 (2020).
- [31] Y. Wang, I. Esterlis, T. Shi, J. I. Cirac, and E. Demler, Zero-temperature phases of the two-dimensional hubbard-holstein model: A non-gaussian exact diagonalization study, *Phys. Rev. Res.* **2**, 043258 (2020).
- [32] Z. Han, S. A. Kivelson, and H. Yao, Strong coupling limit of the holstein-hubbard model, *Phys. Rev. Lett.* **125**, 167001 (2020).
- [33] M. Weber and J. K. Freericks, Real-time evolution of static electron-phonon models in time-dependent electric fields, *Phys. Rev. E* **105**, 025301 (2022).
- [34] D. Jansen, J. Bonča, and F. Heidrich-Meisner, Finite-temperature optical conductivity with density-matrix renormalization group methods for the holstein polaron and bipolaron with dispersive phonons, *Phys. Rev. B* **106**, 155129 (2022).
- [35] M. R. Carbone, S. Fomichev, A. J. Millis, M. Berciu, D. R. Reichman, and J. Sous, [The generalized green's function cluster expansion: A python package for simulating polarons](#) (2022).
- [36] A. Götz, S. Beyl, M. Hohenadler, and F. F. Assaad, Valence-bond solid to antiferromagnet transition in the two-dimensional su-schrieffer-heeger model by langevin dynamics, *Phys. Rev. B* **105**, 085151 (2022).
- [37] S. Li and S. Johnston, Suppressed superexchange interactions in the cuprates by bond-stretching oxygen phonons (2022), [arXiv:2205.12678 \[cond-mat.str-el\]](#).
- [38] W. Barford and R. J. Bursill, Effect of quantum lattice fluctuations on the peierls broken-symmetry ground state, *Phys. Rev. B* **73**, 045106 (2006).
- [39] A. Nocera, J. Sous, A. E. Feiguin, and M. Berciu, Bipolaron liquids at strong peierls electron-phonon couplings, *Phys. Rev. B* **104**, L201109 (2021).
- [40] [URL\\_will\\_be\\_inserted\\_by\\_publisher.](#)
- [41] S. R. White, Density matrix formulation for quantum renormalization groups, *Phys. Rev. Lett.* **69**, 2863 (1992).
- [42] S. R. White, Density-matrix algorithms for quantum renormalization groups, *Phys. Rev. B* **48**, 10345 (1993).
- [43] U. Schollwöck, The density-matrix renormalization group, *Rev. Mod. Phys.* **77**, 259 (2005).
- [44] E. V. L. de Mello and J. Ranninger, Dynamical properties of small polarons, *Phys. Rev. B* **55**, 14872 (1997).
- [45] C. Zhang, E. Jeckelmann, and S. R. White, Dynamical properties of the one-dimensional holstein model, *Phys. Rev. B* **60**, 14092 (1999).
- [46] L. Mathey and D.-W. Wang, Phase diagrams of one-dimensional bose-fermi mixtures of ultracold atoms, *Phys. Rev. A* **75**, 013612 (2007).
- [47] G. Xianlong, M. Rizzi, M. Polini, R. Fazio, M. P. Tosi, V. L. Campo, and K. Capelle, Luther-emery phase and

- atomic-density waves in a trapped fermion gas, *Phys. Rev. Lett.* **98**, 030404 (2007).
- [48] M. Berciu, Green's function of a dressed particle, *Phys. Rev. Lett.* **97**, 036402 (2006).
- [49] G. L. Goodvin and M. Berciu, Momentum average approximation for models with electron-phonon coupling dependent on the phonon momentum, *Phys. Rev. B* **78**, 235120 (2008).
- [50] M. Berciu and H. Fehske, Momentum average approximation for models with boson-modulated hopping: Role of closed loops in the dynamical generation of a finite quasiparticle mass, *Phys. Rev. B* **82**, 085116 (2010).
- [51] D. J. J. Marchand, G. De Filippis, V. Cataudella, M. Berciu, N. Nagaosa, N. V. Prokof'ev, A. S. Mishchenko, and P. C. E. Stamp, Sharp transition for single polarons in the one-dimensional su-schrieffer-heeger model, *Phys. Rev. Lett.* **105**, 266605 (2010).
- [52] O. Penrose and L. Onsager, Bose-einstein condensation and liquid helium, *Phys. Rev.* **104**, 576 (1956).
- [53] C. N. Yang, Concept of off-diagonal long-range order and the quantum phases of liquid he and of superconductors, *Rev. Mod. Phys.* **34**, 694 (1962).
- [54] N. D. Mermin and H. Wagner, Absence of ferromagnetism or antiferromagnetism in one- or two-dimensional isotropic heisenberg models, *Phys. Rev. Lett.* **17**, 1133 (1966).
- [55] N. D. Mermin, Absence of ordering in certain classical systems, *Journal of Mathematical Physics* **8**, 1061 (1967).
- [56] S. Rombouts, D. van Neck, K. Peirs, and L. Pollet, Maximum occupation number for composite boson states, *Modern Physics Letters A* **17**, 1899 (2002), <https://doi.org/10.1142/S0217732302008411>.
- [57] M. Combescot, O. Betbeder-Matibet, and F. Dubin, The many-body physics of composite bosons, *Physics Reports* **463**, 215 (2008).
- [58] W. P. Su, J. R. Schrieffer, and A. J. Heeger, Solitons in polyacetylene, *Phys. Rev. Lett.* **42**, 1698 (1979).
- [59] E. Jeckelmann and S. R. White, Density-matrix renormalization-group study of the polaron problem in the holstein model, *Phys. Rev. B* **57**, 6376 (1998).
- [60] C. Brockt, F. Dorfner, L. Vidmar, F. Heidrich-Meisner, and E. Jeckelmann, Matrix-product-state method with a dynamical local basis optimization for bosonic systems out of equilibrium, *Physical Review B* **92**, 10.1103/physrevb.92.241106 (2015).
- [61] S. Mardazad, Y. Xu, X. Yang, M. Grundner, U. Schollwöck, H. Ma, and S. Paeckel, Quantum dynamics simulation of intramolecular singlet fission in covalently linked tetracene dimer, *The Journal of Chemical Physics* **155**, 194101 (2021).
- [62] J. Haegeman, J. I. Cirac, T. J. Osborne, I. Pižorn, H. Verschelde, and F. Verstraete, Time-dependent variational principle for quantum lattices, *Physical Review Letters* **107**, 10.1103/physrevlett.107.070601 (2011).
- [63] J. Haegeman, C. Lubich, I. Oseledets, B. Vandereycken, and F. Verstraete, Unifying time evolution and optimization with matrix product states, *Physical Review B* **94**, 10.1103/physrevb.94.165116 (2016).
- [64] A. J. Daley, C. Kollath, U. Schollwöck, and G. Vidal, Time-dependent density-matrix renormalization-group using adaptive effective hilbert spaces, *Journal of Statistical Mechanics: Theory and Experiment* **2004**, P04005 (2004).
- [65] M. Zwolak and G. Vidal, Mixed-state dynamics in one-dimensional quantum lattice systems: A time-dependent superoperator renormalization algorithm, *Phys. Rev. Lett.* **93**, 207205 (2004).
- [66] S. R. White and A. E. Feiguin, Real-time evolution using the density matrix renormalization group, *Phys. Rev. Lett.* **93**, 076401 (2004).
- [67] C. Hubig, I. P. McCulloch, U. Schollwöck, and F. A. Wolf, Strictly single-site DMRG algorithm with subspace expansion, *Physical Review B* **91**, 10.1103/physrevb.91.155115 (2015).